Design considerations of form birefringent microstructures

Ivan Richter, Pang-Chen Sun, Fang Xu, and Yeshayahu Fainman

Diffraction characteristics of high-spatial-frequency (HSF) gratings are evaluated for application to polarization-selective computer-generated holograms by the use of two different approaches: second-order effective-medium theory (EMT) and rigorous coupled-wave analysis (RCWA). The reflectivities and the phase differences for TE- and TM-polarized waves are investigated in terms of various input parameters, and results obtained with second-order EMT and RCWA are compared. It is shown that although the reflection characteristics can be accurately modeled with the second-order EMT, the phase difference created by form birefringence for TE- and TM-polarized waves requires the use of a more rigorous, RCWA approach. The design of HSF gratings in terms of their form birefringence and reflectivity properties is discussed in conjunction with polarization-selective computer-generated holograms. A specific design optimization example furnishes a grating profile that provides a trade-off between the largest form birefringence and the lowest reflectivities.

Key words: High-spatial-frequency gratings, form birefringence, effective-medium theory, rigorous coupled-wave analysis, polarization-selective diffractive element.

1. Introduction

Polarization-selective computer-generated holograms (CGH's) or birefringent CGH's (BCGH's) have been found to be useful for numerous applications such as image processing, photonic switching, and packaging optoelectronic devices and systems.[1,2] In contrast to a conventional CGH, which is polarization insensitive, the BCGH is capable of implementing two completely different functions for the two orthogonal polarizations. Originally[1,2] these BCGH's were composed of surface-relief gratings fabricated in two substrates, with at least one of them birefringent. All surfaces of the BCGH elements were coated with an antireflection (AR) layer to minimize the insertion losses.[2] To improve the performance, increase the reliability, decrease the fabrication errors, and allow low cost and manufacturability, we consider a single-substrate BCGH that utilizes form birefringence and AR properties of high-spatial-frequency (HSF) gratings. Consider two approaches to constructing a single-substrate BCGH: (1) create a surface-relief etch in an isotropic substrate with posterior fabrication of the HSF form birefringent gratings in each phase level, or (2) create the form birefringent grating overcast by a layer of photoresist with a posterior-fabricated surface-relief etch. In this paper, motivated by the advantages of a single-substrate BCGH, we focus on the investigation of HSF gratings in terms of design and optimization of their form birefringence and AR properties.

HSF gratings with periodicities much smaller than the wavelength of incident light have been studied[3–6] because of their many unique and interesting properties that distinguish them from other diffraction gratings. The general behavior of a HSF grating appears to be similar to that of thin films[3] because only the zeroth diffracted order is allowed to propagate. Hence HSF gratings can be used as alternatives for single or multiple layers of thin films, allowing more flexibility in design and fabrication processes. Unlike bulk birefringence, which is caused by anisotropic electrical properties on a microscopic scale, form birefringence arises on scales much larger compared with these microscopic dimensions but smaller than the wavelength of incoming light.[7] The form birefringence phenomenon can be characterized by the phase difference obtained between the transmit-

The authors are with the Department of Electrical and Computer Engineering, University of California at San Diego, La Jolla, California 92093-0407. I. Richter is on leave from the Department of Physical Electronics, Faculty of Nuclear Sciences and Physical Engineering, Czech Technical University in Prague, 115 19 Prague 1, Czech Republic.

Received 19 September 1994; revised manuscript received 29 November 1994.

0003-6935/95/142421-09$06.00/0.

ted TE- and TM-polarized light waves, similar to the optical anisotropy observed in a slab of a uniaxial crystal. This anisotropic effect can be used for phase retardation, as in retardation plate devices,[8] or for distributed index structures to imitate a sawtooth grating.[9] Furthermore, because of their polarization-selectivity properties, such structures can be used as polarizing beam splitters,[10,11] Another important feature of HSF gratings is their AR property. Compared with standard optical thin-film coating technologies, the HSF AR microstructure provides the advantages of durability, damage resistivity, and the ability to substitute materials of specific characteristics that are unsuitable or unavailable in thin-film form.

Mainly two approaches are used for modeling HSF microstructures. The first approach, which is called the effective-medium theory (EMT), solves the grating diffraction problem by dividing the grating profile into a stack of multiple layers and substituting each layer with a homogeneous anisotropic material of equivalent dielectric constants for a normal incidence TE-polarized field (electric-field vector perpendicular to the grating vector, or $E \perp K$) or TM-polarized field[12,13] (electric field parallel to the grating vector, or $E \parallel K$). Because only the zeroth diffractive order is assumed to propagate, the optical properties of the HSF grating are determined by the use of wave propagation in stratified media. The second approach is based on rigorous electromagnetic wave theory, known as differential[14,15] and integral methods.[14] The design approach we used in this paper is based on a differential method that is called the rigorous coupled-wave analysis[16,17] (RCWA).

This paper has two main objectives: The first is to provide a detailed comparison between EMT and RCWA approaches to characterize the form birefringence and the reflectivity of HSF gratings. For various input parameters we show that EMT, compared with RCWA, can provide accurate results for reflectivities, but results obtained for a phase difference between TE- and TM-polarized waves deviate significantly. This confirms the necessity of using RCWA for a single-substrate BCGH design, which requires high accuracy for encoding the desired phase differences. The second objective is to establish simple criteria for defining the grating profile to satisfy two design considerations of HSF microstructures for a single-substrate BCGH: a large phase difference and low as well as uniform reflectivities for both TE and TM polarizations. This design criteria set a trade-off between two extreme grating-shape cases, the rectangular and the triangular profile gratings.

In Section 2 we briefly describe the EMT and the RCWA techniques used for a HSF grating design, together with the chosen computation algorithm. In Section 3 we compare and discuss numeric simulation results obtained from the EMT and RCWA for phase differences and reflectivities of gratings with various parameters. Section 4 introduces the design criteria of HSF gratings for BCGH application, providing an optimal HSF grating profile that can furnish the largest birefringence and smallest reflectivities. Section 5 summarizes the results.

2. Effective-Medium Theory and Rigorous Coupled-Wave Analysis

The EMT model[12,13,18,19] is based on the uniaxial of a HSF grating. Such a grating has a small period-to-wavelength ratio such that high diffraction orders are evanescent and only the zeroth order can propagate. A surface-relief grating of a rectangular-groove profile, as shown in Fig. 1(a), can be divided into three regions: the region of incident material, the grating region, and the substrate region. The regions of incident and substrate materials are homogeneous isotropic dielectric, with real dielectric constants ϵ_{I} and ϵ_{III}, respectively. The grating region consists of both materials, divided from each other by the boundary of the microstructure, defined as a grating profile. Here, d is the grating thickness, Λ is the grating period, F is the duty cycle (filling factor) of the grating, $\mathbf{K} = 2\pi\hat{x}/\Lambda$ is the grating vector parallel to the $\hat{x}$ axis, and $k = |\mathbf{k}| = 2\pi/\lambda$ is the magnitude of the incident wave vector. A normally incident electromagnetic wave of wavelength λ is either TE polarized or TM polarized. Figure 1(b) illustrates the correspondent thin-film equivalent of the grating in Fig. 1(a), represented by a single homogeneous anisotropic layer with the same thickness d and with the corresponding effective dielectric constants $\epsilon_{E\perp K}$ for $\epsilon_{E\parallel K}$ for TE and TM polarizations, respectively. Similarly, an arbitrary grating profile [see Fig. 2(a)] can be modeled by a stack of thin layers [Fig. 2(b)] with the total thickness identical to the grating-

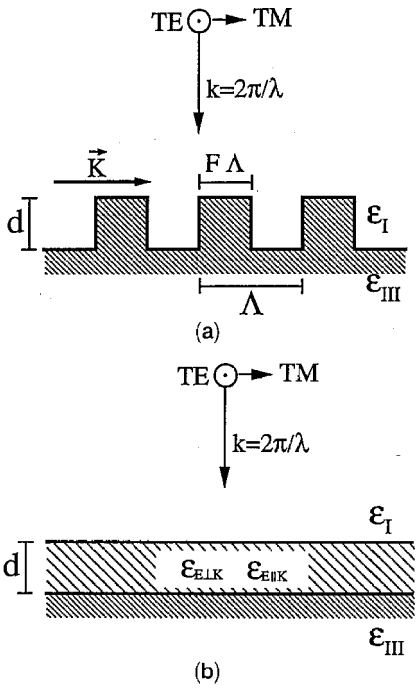

Fig. 1. Schematic diagram of (a) a HSF rectangular surface-relief grating, (b) its equivalent homogeneous layer model.

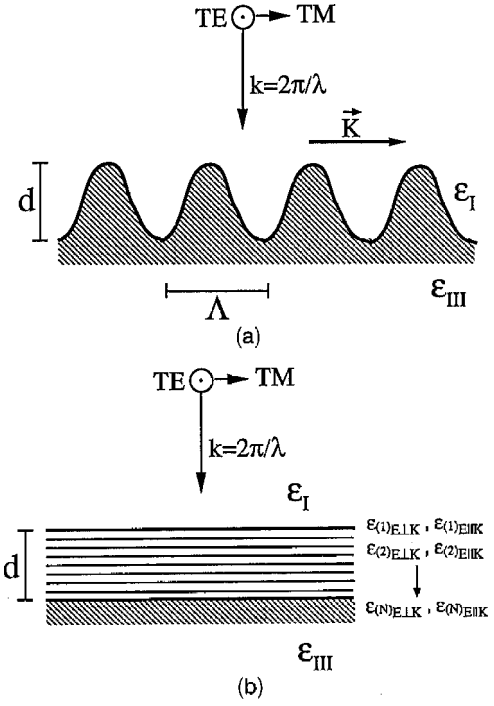

Fig. 2. Schematic diagram of (a) HSF sinusoidal surface-relief grating, (b) its equivalent homogeneous multilayer model.

region thickness but with different equivalent dielectric constants for each layer: $\epsilon_{E\perp K}^{(i)}$, and $\epsilon_{E\|K}^{(i)}$, where $i = 1, \ldots, N$, N being the number of layers.

In general, $\epsilon_{E\perp K}$ and $\epsilon_{E\|K}$ are determined by the solution of the transcendental equations[12] derived under the conditions of normal incidence and nonstatic electromagnetic-field distribution in the grating structure. As the period-to-wavelength ratio Λ/λ becomes larger, more higher-order terms from the series expansions of transcendental functions must be included in the analysis. Zero-order approximation[7] is independent of Λ/λ and can be obtained under the assumption that the electric field **E** (for $E \perp K$ polarization) and the displacement vector **D** (for $E \| K$ polarization) are approximately constant across the grating period:

$$\epsilon_{0,E\perp K} = F\epsilon_{\mathrm{III}} + (1 - F)\epsilon_{\mathrm{I}},$$
$$\epsilon_{0,E\|K} = \frac{\epsilon_{\mathrm{III}}\epsilon_{\mathrm{I}}}{F\epsilon_{\mathrm{I}} + (1 - F)\epsilon_{\mathrm{III}}}, \qquad (1)$$

where F is the duty cycle of the grating and the subscript 0 indicates the zero-order approximation. In our numerical simulation, however, more precise second-order solutions are used[12,13]:

$$\epsilon_{2,E\perp K} = \epsilon_{0,E\perp K} + \frac{1}{3}\left(\frac{\Lambda}{\lambda}\right)^2 \pi^2 F^2(1 - F)^2(\epsilon_{\mathrm{III}} - \epsilon_{\mathrm{I}})^2,$$
$$\epsilon_{2,E\|K} = \epsilon_{0,E\|K} + \frac{1}{3}\left(\frac{\Lambda}{\lambda}\right)^2 \pi^2 F^2(1 - F)^2\left(\frac{1}{\epsilon_{\mathrm{III}}} - \frac{1}{\epsilon_{\mathrm{I}}}\right)^2$$
$$\times \epsilon_{0,E\|K}^3\epsilon_{0,E\perp K}, \qquad (2)$$

where $\epsilon_{0,E\perp K}$ and $\epsilon_{0,E\|K}$ are defined in Eqs. (1). The second-order effective dielectric constants [Eqs. (2)], in contrast to the zero-order ones [Eqs. (1)], depend on the square of the Λ/λ ratio. Equations (1) and Eqs. (2) are designated as the zeroth-order EMT and the second-order EMT, respectively. The properties of the single or multiple layers replacing the grating region are obtained by the use of classical methods of wave propagation in stratified media.[20]

Although the zeroth- and the second-order EMT's, as presented below, were shown to give precise results for $\Lambda/\lambda \ll 1$, they are not valid when the value of Λ/λ approaches $(\sqrt{\epsilon_{\mathrm{I}}} + \sqrt{\epsilon_{\mathrm{III}}})^{-1}$, as EMT is based on the premise that only zero orders are propagating. On the other hand, RCWA's, although usually very intensive in their numeric implementations, can accurately describe the diffraction by surface-relief gratings for arbitrary period-to-wavelength ratios. The RCWA is one of the rigorous methods[14] whereas other rigorous techniques, such as finite-difference,[21] finite-element,[22] as well as integral[14] and modal[23] methods, have also been successfully used. For our study, RCWA was chosen as the most developed and suitable modeling approach.

The RCWA, first introduced in Ref. 16 to analyze the diffraction properties of TE-polarized light in lossless surface-relief gratings, can be summarized as follows. A single period of a surface-relief grating is first divided into a large number of planar layers, as depicted in Fig. 3. For each such layer, the optical fields are formulated in terms of spatial harmonics by Fourier series expansions of the dielectric constant. The effective dielectric constant of each layer is calculated as a volume-weighted average of the dielectric constants of the incident and the substrate regions. When the components of these spatial harmonics are substituted into the wave equation, a sequence of coupled first-order linear differential equations can be generated. The equations can be solved in terms of their eigensolutions. The field distribution in each layer of the grating can be represented by the superposition of these eigensolutions. Transmission and reflection diffractive fields can then be derived by a match of the appropriate

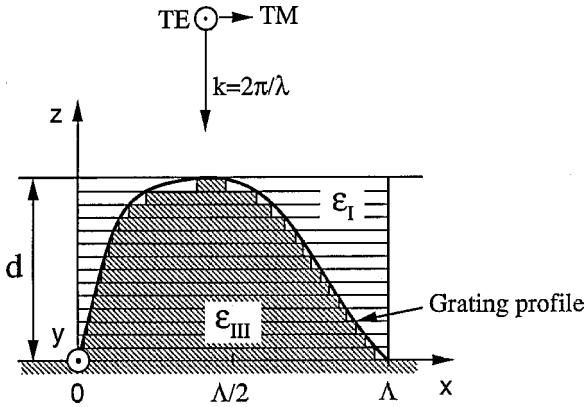

Fig. 3. Geometry of surface-relief grating and its decomposition into thin rectangular gratings by RCWA.

boundary conditions. Subsequently, diffraction efficiencies are calculated for propagating transmitted and reflected diffraction orders. Energy conservation is used as a criterion for the convergence of numeric solutions. Input parameters, namely the total number of diffraction orders and the number of layers, are increased until the precision and the results themselves remain constant within the limits of the chosen numeric accuracy. The case of TM light polarization was treated in a similar manner, with the proper wave equation used for this polarization and the coupled-wave equations modified for the case of a surface-relief grating.[17] The RCWA was also extended and generalized to more complicated cases.[24–27]

In our own implementation of the original algorithm, the problem of instability was encountered, especially for materials with a larger effective grating thickness characterized by d, ϵ_I, and ϵ_{III}. The instability is caused primarily by the large linear system coefficients, which contain exponential factors with the exponent given by the product of eigenvalue and grating thickness. Unfortunately, this would exactly be the case of a deep, highly formed birefringent grating that would be required for constructing a single-substrate BCGH. Thus, to avoid numeric calculations instabilities, a modified algorithm for solving the boundary conditions, as recently presented in Ref. 28, was successfully implemented. If the eigenvalues are suitably reorganized and resorted, as in Ref. 28, it is possible to find a recurrent definition for a new sequence of matrices that will behave well, even for large effective grating thicknesses or a large number of included diffraction orders.

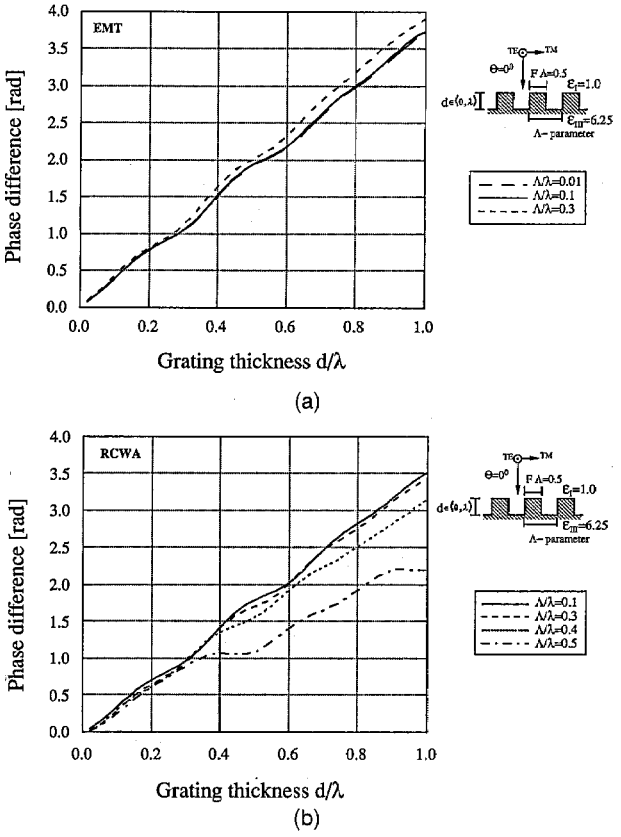

Fig. 4. Phase difference between TE- and TM-polarized light at normal incidence as a function of a normalized thickness rectangular-shaped grating of 50% duty cycle, with the normalized grating period as a parameter, with (a) second-order EMT, (b) RCWA. The grating is made of a material with $\epsilon_{III} = 6.25$ in air $\epsilon_I = 1.0$.

3. Numeric Simulations and Comparison

One of the objectives of this paper is to compare the TE and the TM wave phase differences and reflectivity characteristics of HSF gratings calculated with the EMT and RCWA and to determine when it is possible to rely on the results obtained from the use of EMT and when it is necessary to use RCWA. Below, the phase difference between transmitted TE- and TM-polarized waves and reflectivities for TE and TM polarizations are calculated as a function of different HSF grating parameters, including certain grating profiles, grating thicknesses, angles of incidence, and duty cycles. To carry out the comparison, we have chosen $\epsilon_I = 1.0$ and $\epsilon_{III} = 6.25$ for all calculations presented.

A. Phase Difference between TE- and TM-Polarized Waves

Form birefringence of HSF gratings is characterized by the phase difference between TE- and TM-polarized waves propagating through the grating. Figure 4 shows the phase difference as a function of normalized grating thickness (d/λ), with a normalized grating period as a parameter (Λ/λ), when the incident wave propagates normal to the grating surface. Such normalization of parameters is kept throughout this paper. The grating profile is rectangular, with a 50% duty cycle. Figure 4(a) shows results from the second-order EMT whereas, in comparison, Fig. 4(b) shows results from the RCWA. In both figures, the phase difference increases almost linearly, with slow modulation depending on the grating depth. This modulation is characterized by ripples on curves in Figs. 4(a) and 4(b), which are due to multiple reflections inside the grating structure, similar to that of the thin-film case. The results from the second-order EMT [Fig. 4(a)] do not exactly match those obtained with RCWA [Fig. 4(b)] in which difference between them gradually increases for a larger grating period. RCWA results show that the phase difference decreases when Λ/λ increases (for constant d/λ), whereas the EMT results show an opposite behavior. The deviation becomes more pronounced when Λ/λ is greater than 0.4 because the EMT does not account for higher propagating diffractive orders.

Figure 5 illustrates the phase difference introduced by the rectangular grating as a function of its duty cycle F for several normalized grating periods $(\Lambda/\lambda = 0.1, 0.2, 0.3)$ and a fixed grating depth $(d/\lambda = 1.0)$. The phase difference for different duty cycles is not symmetrical, with its maximum value located aside the 50% duty cycle. When the grating

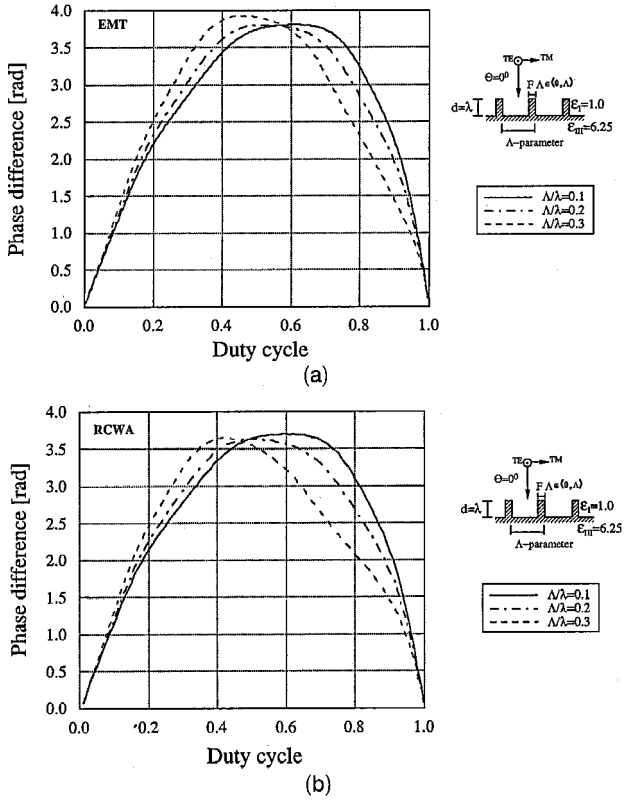

Fig. 5. Phase difference between TE- and TM-polarized light at normal incidence as a function of a rectangular-shaped grating duty cycle, with $d/\lambda = 1.0$ and Λ/λ as a parameter, with (a) second-order EMT, (b) RCWA.

period is increased, the location of the maximum phase difference shifts toward smaller F values. Comparing the results obtained with the EMT [Fig. 5(a)] and the RCWA [Fig. 5(b)], we observe that the values provided by the EMT are always slightly higher than these provided by the RCWA.

Figure 6 depicts the phase differences for the rectangular 50% duty cycle HSF grating as a function of incidence angle. For this special case, the plane of incidence contains the grating wave vector, with angle θ between the wave propagation direction and the surface normal (see Fig. 6 for the definitions of TE and TM polarizations). For $\Lambda/\lambda = 0.1$, the EMT and the RCWA results follow the same functional behavior, i.e., the phase difference decreases with the increase of the angle of incidence. However, for $\Lambda/\lambda = 0.3$, the results from the EMT and the RCWA are different: EMT results show behavior similar to that with $\Lambda/\lambda = 0.1$, whereas RCWA results show opposite behavior, in which the phase difference increases with the increase of the incident angle. The recent study of Ref. 29 shows that when the HSF grating is illuminated under an angle, the anisotropic nature of the HSF grating needs to be taken into consideration for calculating the effective indices from the EMT, especially when Λ/λ approaches the nonquasi-static regime [i.e., $\Lambda/\lambda \rightarrow (\sqrt{\epsilon_I} + \sqrt{\epsilon_{III}})^{-1}$]. This may explain the large difference between the results obtained from use of the EMT and the RCWA at $\Lambda/\lambda = 0.3$ (see Fig. 6). In all cases, the phase differences remain almost constant for small incidence angles (i.e., less than 1.5% deviation in the range 0°–20°). This angular behavior needs to be accounted for in designs of BCGH for applications that operate wide angular bandwidth signals.

Similarly, we can model more complicated surface-relief microstructures (e.g., triangular shaped). Figure 7 shows the phase differences for triangular profiles as a function of normalized grating thickness with grating periods of $\Lambda/\lambda = 0.1$ and 0.3, calculated with the EMT and the RCWA. For both grating profiles, the phase difference dependence is close to a linear function, similar to that of the rectangular profile (see Fig. 4), but with a smaller slope and much less modulation. Results from the EMT and the RCWA are close to each other when $\Lambda/\lambda = 0.1$ but they are different for an increased ratio of $\Lambda/\lambda = 0.3$.

B. Reflectivity

The second HSF grating property of interest for our design is reflectivity for both TE and TM polarizations. Figure 8 shows zero-order reflectivities as a function of grating depth for a 50% duty cycle rectangular grating with periods of $\Lambda/\lambda = 0.1$ and 0.3. The reflectivity functions have sinusoidal behavior, with periodicities of oscillations different for TE and TM

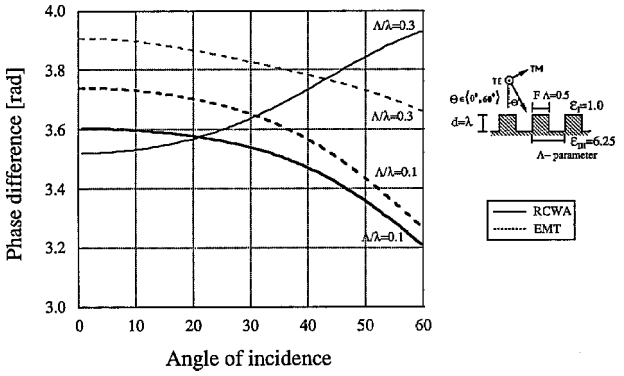

Fig. 6. Phase difference between TE- and TM-polarized light as a function of angle of incidence for a rectangular 50% duty cycle grating with $d/\lambda = 1.0$ and $\Lambda/\lambda = 0.1$ and 0.3.

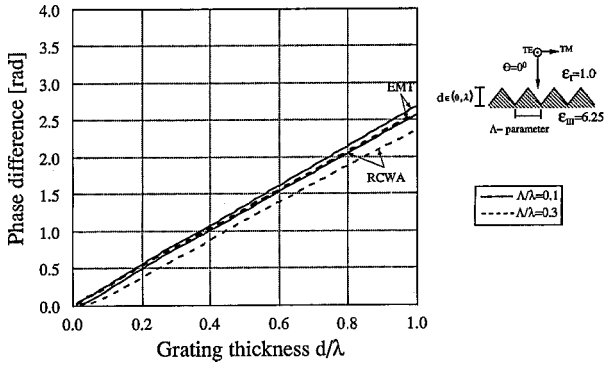

Fig. 7. Comparison of phase differences between TE- and TM-polarized light at normal incidence as a function of normalized thickness, and normalized grating period as a parameter for a triangular profile grating.

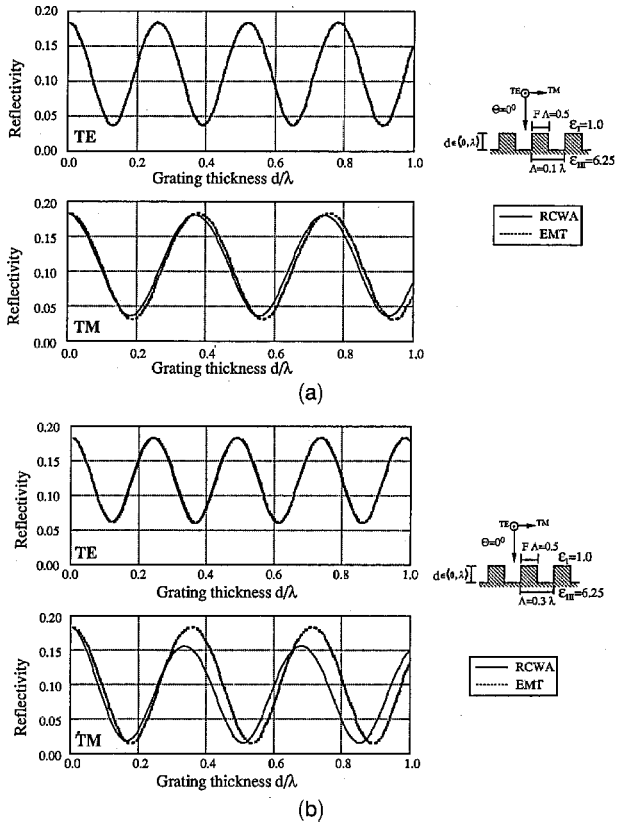

Fig. 8. Reflectivity of TE- and TM-polarized light at normal incidence as a function of a normalized thickness rectangular-shaped grating of 50% duty cycle for (a) $\Lambda/\lambda = 0.1$, (b) $\Lambda/\lambda = 0.3$.

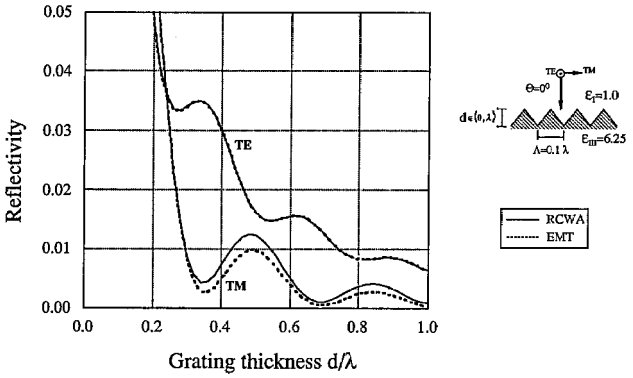

Fig. 9. Comparison of reflectivities of TE- and TM-polarized light at normal incidence as a function of a normalized triangular-shaped grating thickness and $\Lambda/\lambda = 0.1$.

polarizations because of different effective dielectric constants. Although this characteristic can be used, for example, for polarization-selective mirrors,[30] it is undesirable for our design of a single-substrate BCGH, for which low and uniform reflectivities for both polarizations are required. Both Figs. 8(a) and 8(b) indicate that the EMT and the RCWA produce similar results in a HSF grating, with one exception occurring for TM polarization with $\Lambda/\lambda = 0.3$, in which approximately 11% difference in maximum reflectivity occurs for calculations obtained from the EMT and the RCWA.

Reflection properties for triangular profiles with $\Lambda/\lambda = 0.1$ are shown in Fig. 9 for TE and TM polarization. To show the results in detail, the y axis was scaled up. Unlike the rectangular grating (Fig. 8), which exhibits large reflectivity oscillations in grating depth, reflectivities for both triangular gratings decline rapidly as grating depth increases, exhibiting damped oscillatory behavior. Therefore both reflectivities start to stabilize and stay within a low value after reaching a certain grating thickness. For a triangular grating with $\Lambda/\lambda = 0.1$ and $d/\lambda > 0.75$, the reflectivities for both TE and TM polarizations are less than 1%. Thus it can be utilized as a substitution for antireflective coatings. In particular the triangular profile microstructure exhibits smaller reflectivity and less oscillations, which will be shown useful in designing HSF gratings for a single-substrate BCGH.

In conclusion, results presented in this section for rectangular-shaped gratings show that the EMT provides quite accurate results for reflectivities at TE ($E \perp K$) polarization for both $\Lambda/\lambda = 0.1$ and 0.3 (see Fig. 8). However, for the reflectivity at TM ($E \parallel K$) polarization, the difference between the results of the EMT and the RCWA is negligibly different for $\Lambda/\lambda \leq 0.1$ [see Fig. 8(a)]. This difference in TM wave reflectivity becomes even more pronounced for $\Lambda/\lambda = 0.3$ [see Fig. 8(b)] because of the larger errors in calculating the effective refractive index with the EMT. This confirms the conclusions from the literature,[13,18,19] i.e., that EMT provides an accurate, efficient and simple tool that is useful for modeling and designing AR microstructures. In contrast, large deviations were found for phase difference results obtained with the EMT and the RCWA. For example, the phase calculation error from using the EMT instead of the RCWA can exceed 10% (see Fig. 4 at $\Lambda/\lambda = 0.3$ and $d/\lambda = 1.0$), whereas a 16-phase-level CGH corresponds to a phase quantization level of 6.3%. Therefore, the EMT calculations can introduce an error bigger than the quantization error. These deviations are especially pronounced for gratings with larger grating periods, which are easier to fabricate, and thus are more attractive for our design. Therefore, when phase properties of HSF gratings are of critical importance (e.g., single-substrate BCGH design), we found that a rigorous technique (e.g., RCWA) is necessary to guarantee correct results.

4. Design Considerations of High-Spatial-Frequency Gratings for a Birefringent Computer-Generated Hologram

The coexistence of form birefringence and AR properties in HSF gratings creates a new dimension in design of optical birefringent components. With HSF gratings such components can be designed and fabricated by either optical casting or direct etching the grating structures into the substrate.[8] Unlike the anisotropic thin film that exhibits fixed birefringence, the birefringence of the HSF grating microstructure

can be controlled by change in one of the grating parameters. For example, the surface profile or duty cycle can be varied to tune the birefringence according to the design requirements. In addition to possessing form birefringence, the HSF microstructures possess AR characteristics that can also be considered and used in designing optical components. However, because the birefringence and the AR properties of HSF microstructures are interrelated, design optimization will be required for applications that rely on both properties (e.g., a single-substrate BCGH).

Despite the advantages in design flexibility discussed above, fabricating such a HSF microstructure with a feature size smaller than the wavelength remains a challenging task. The fabrication difficulties are especially pronounced for HSF gratings that need to be operated in the visible wavelength region, where the grating feature size is reduced to submicrometer range. Existing techniques, such as holographic recording with subsequent reactive ion etching[6] or x-ray lithography,[4] can provide a minimum feature size close to this range, not, however, without losing the grating-shape design flexibility and accuracy. Current advances in developing microfabrication technology show promise for fabrication of HSF microstructures of a certain profile in the visible wavelength range.

For the design of a single-substrate BCGH, we require maximized phase difference and minimized reflectivity for TE- and TM-polarized waves. As illustrated in Fig. 3, any arbitrary grating profile can be divided into multiple layers, each consisting of an effective rectangular grating that approximates the actual profile. To maximize the phase difference of the HSF microstructure, the phase difference of each individual layer should be maximized. Figure 5 shows that the phase difference for TE and TM waves can vary in a wide range, depending on the duty cycle of the HSF grating. Consider a triangular grating decomposed into layers with approximately rectangular shape. As the duty cycles of these effective rectangular gratings change linearly from zero to one throughout the entire triangular grating depth, the total phase difference obtained with a triangular HSF microstructure will be smaller than the phase difference provided by an equal thickness HSF rectangular-shaped grating with a 50% duty cycle.

In contrast, the triangular profile HSF grating exposes much smaller and more uniform reflection [Fig. 10(b)] than the rectangular one, because its profile can be represented by layers with a monotonically increasing average dielectric constant. The rectangular profile, though, has the same average dielectric constant for each individual layer, resulting in a large dielectric constant discontinuity at the bottom and the top of the grating[6] and consequently exhibits strong oscillations in reflectivity, depending on the grating depth (Fig. 8). Although at certain depths or duty cycles the rectangular grating can also provide very low reflectivities for both TE and TM polarizations, for practical purposes, especially because of the limits of current fabrication techniques, such strong dependence of reflection on the grating depth is not acceptable.

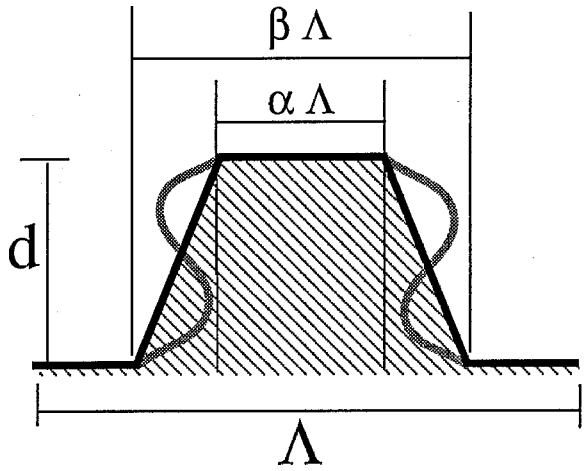

Fig. 10. Schematic drawing of the optimized profile that comprises a large phase difference (curved shape) and a simultaneous low and uniform reflectivity (trapezoidal shape).

It can be concluded that designing a HSF grating that possesses both qualities, i.e., a large phase difference and low and uniform reflectivities for both TE and TM polarizations, requires another grating shape lying between the rectangular and the triangular profiles. Below, simple design criteria that allow us to define an optimum HSF grating profile for achieving the necessary HSF grating properties is specified. When these criteria are applied, numeric results based on RCWA are provided.

The first criterion defines a range of duty cycles that can be obtained with multiple layers representing the grating profile (see Fig. 3). From Fig. 5(b), we first locate the position for the maximum phase difference (e.g., for $\Lambda/\lambda = 0.3$, $F = 0.4$); then, on each side of this point, we set two equidistant (without loss of generality) points defined as α and β (see Fig. 10). α and β set the range of duty cycles that can be obtained with the multiple-layer representation of the desired HSF grating profile (i.e., $\alpha < F < \beta$). Depending on the total phase difference required, the distance between α and β can vary within two extreme cases that represent the rectangular grating (40% duty cycle: $\alpha = \beta = 0.4$) and the triangular grating ($\alpha = 0$, $\beta = 1$), respectively. Thus all possible grating shapes (like the curved profile in Fig. 10) that satisfy the criterion mention above are generally allowed.

The second criterion ensures small and uniform reflectivities independent of grating thickness for grating profiles that satisfy the first criterion. This requires that the effective dielectric constants that correspond to the multiple layers that represent the HSF grating should be a monotonically decreasing sequence, implying an increase in groove width from the bottom to the top of the grating. Here, among all possible grating profiles within the limits α and β, a

linear function was chosen for simplicity, as shown in Fig. 10. More complicated functions could be treated in a similar manner. In summary, the actual geometric shape of the grating profile now depends on the two parameters α and β. Varying these two parameters will allow us to find the optimum grating shape that will satisfy specific requirements on the phase difference and the reflectivity properties.

The results from RCWA, which compare the profiles with different parameters α and β for $\Lambda/\lambda = 0.3$, are shown in Figs. 11 and 12 for the phase difference and the reflectivity, respectively. The phase differences shown in Fig. 11 decrease from their maximum value for the rectangular profile ($\alpha = \beta = 0.4$) toward the minimum value for the triangular profile ($\alpha = 0, \beta = 1$). The TE and the TM reflectivities shown in Figs. 12(a) and 12(b), respectively, reduce much more rapidly than the corresponding decrease in the phase difference with increasing distance between α and β, especially for gratings of a larger thickness. Moreover, increasing the difference between α and β would reduce the amplitude of oscillations for TE and TM reflectivities. The results in Figs. 11 and 12 show that the maximum phase difference and minimum reflectivities cannot coexist in general. Appropriate values of α and β should be determined during the design procedure, depending on specific application requirements (e.g., desired phase difference and acceptable reflectivities).

As a specific example, consider a single-substrate binary-phase BCGH design. A binary-phase BCGH would require two phase levels, zero and π.[2] As a fabrication constraint, we restrict the etch depth not to exceed the value of the operating wavelength; therefore the grating profiles with parameters $\alpha < 0.1$, and $\beta > 0.7$ (see Fig. 11) will not be able to provide the required π phase difference, although they can possess much lower reflectivities (see Fig. 12). A possible trade-off would be to define the grating profile with parameters $\alpha = 0.2$ and $\beta = 0.6$. This profile can satisfy the desired π phase difference requirement, yet still provide more than twice the reduction in peak reflectivities compared with the rectangular-shaped profile. Moreover, the $-\pi$ phase

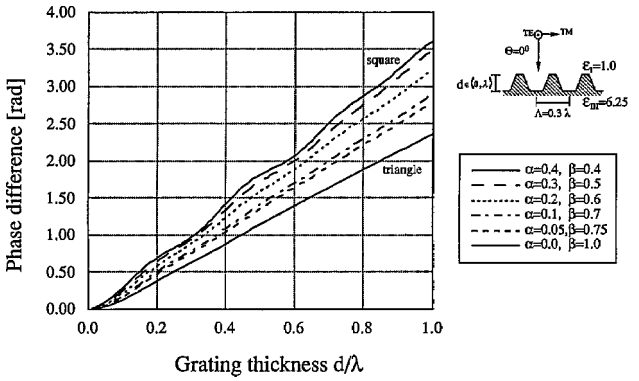

Fig. 11. Phase difference between TE- and TM-polarized light at normal incidence as a function of a normalized thickness optimized profile for $\Lambda/\lambda = 0.3$, obtained by RCWA.

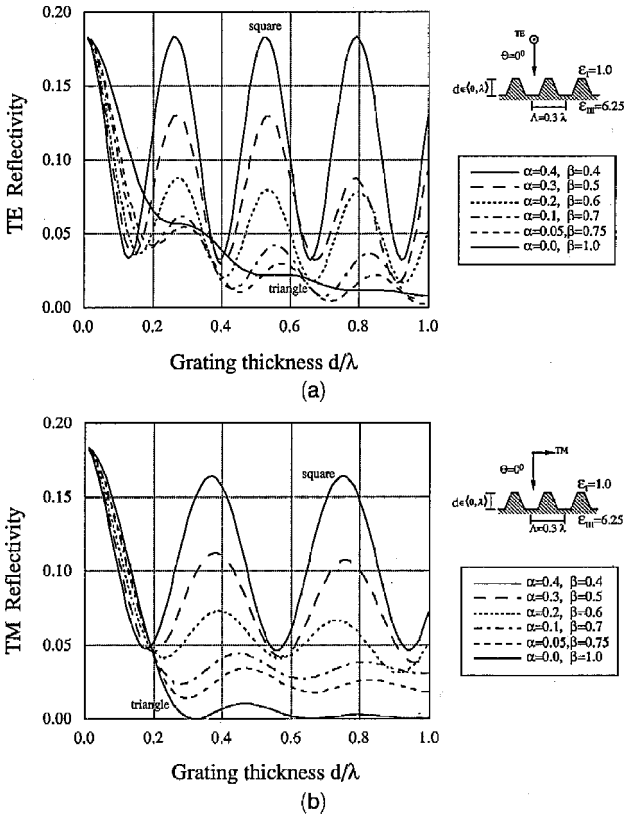

Fig. 12. Reflectivity of (a) TE- and (b) TM-polarized light at normal incidence as a function of normalized thickness optimized profile for $\Lambda/\lambda = 0.3$, obtained by RCWA.

difference can also be achieved simply by the rotation of the grating orientation of 90°. Note that gratings with a larger refractive-index difference ($n_{III} - n_I$) will result in a larger phase difference and reflectivities. Therefore we expect that the design optimization may shift toward a triangular shape for a high refractive-index substrate and toward a rectangular shape for a low refractive-index substrate.

The second desired phase difference for binary BCGH's is zero, which could be simply obtained if no microstructure is used. However, in this case, the surface would exhibit very high reflectivity (see Fig. 12 in the limit of zero grating thickness). For this case, a two-dimensional antireflective microstructure can provide a solution. As shown in Refs. 18 and 31, two-dimensional HSF grating microstructures with identical profiles in both dimensions would exhibit isotropic behavior, resulting in a zero phase difference, while they would give smaller reflectivities than that of the one-dimensional HSF grating.[18] For a single-substrate BCGH, such a HSF microstructure can be obtained by fabrication in the same pixel grating profiles for $+\pi$ and $-\pi$ (i.e., 90° rotated grating) phase differences. Such a structure will result in zero phase difference and minimized reflectivity.

5. Conclusion

The numeric simulation results show that for the HSF grating design for applications that rely on both

reflection and phase difference characteristics, such as a single-substrate BCGH, we need to use the RCWA technique. Detailed comparison between results obtained with the EMT and the RCWA for both the phase difference and the reflectivities for TE and TM polarization have been performed. Although the modeling of reflectivities can be accurately performed by the use of the EMT, as indicated by this and other studies existing in the literature, for phase characteristics a rigorous approach must be used. The influence of changing grating parameters, such as grating thickness, duty cycle, angle of incidence, and HSF grating profile, has also been discussed.

Design considerations of HSF gratings for the possible use in a single-substrate BCGH have been also presented. Two major requirements on HSF gratings are imposed by BCGH application: a large phase difference (form birefringence) and minimum reflectivity for both TE- and TM-polarized light. Although these two performance characteristics are found to be contradictory, we formulated simple design criteria of an optimum grating profile that can provide the desired phase difference and simultaneously reduce the reflectivity. This technique can be used to optimize properties of HSF gratings according to the particular application requirements.

The authors thank J. Ford for his valuable contributions. This work is supported by National Science Foundation grant ECS-9311062, Advance Research Projects Agency-grant OTCII-MDA 972-94-1-002, and NATO 931141.

References

1. J. E. Ford, F. Xu, K. Urquhart, and Y. Fainman, "Polarization-selective computer-generated holograms," Opt. Lett. **18,** 456–458 (1993).
2. F. Xu, J. E. Ford, and Y. Fainman, "Polarization-selective computer-generated holograms: design, fabrication and applications," Appl. Opt. **34,** 256–266 (1995).
3. Y. Ono, Y. Kimura, Y. Ohta, and N. Nishida, "Antireflection effect in ultrahigh spatial-frequency holographic relief gratings," Appl. Opt. **26,** 1142–1146 (1987).
4. D. C. Flanders, "Submicron periodicity gratings as artificial anisotropic dielectrics," Appl. Phys. Lett. **42,** 492–494 (1983).
5. E. Gluch, H. Haidner, P. Kipfer, J. T. Sheridan, and N. Streibl, "Form birefringence of surface relief gratings and its angular dependence," Opt. Commun. **89,** 173–177 (1992).
6. R. C. Enger and S. K. Case, "Optical elements with ultrahigh spatial-frequency surface corrugations," Appl. Opt. **22,** 3220–3228 (1983).
7. M. Born and E. Wolf, *Principles of Optics,* 2nd ed. (Pergamon, Oxford, 1964), Chap. 14, p. 705.
8. L. H. Cescato, E. Gluch, and N. Streibl, "Holographic quarter-wave plates," Appl. Opt. **29,** 3286–3290 (1990).
9. S. Babin, H. Haidner, P. Kipfer, A. Lang, J. T. Sheridan, W. Stork, and N. Streibl, "Artificial index surface relief diffraction optical elements," in *Miniature and Micro-Optics: Fabrication,* C. Roychoudhuri and W. B. Veldkamp, Proc. Soc. Photo-Opt. Instrum. Eng. **1751,** 202–213 (1992).
10. K. Shiraishi, T. Sato, and S. Kawakami, "Experimental verification of a form birefringence polarization splitter," Appl. Phys. Lett. **58,** 211–212 (1991).
11. S. Aoyama and T. Yamashita, "Grating beam splitting polarizer using multi-layer resist method," in *International Conference on the Application and Theory of Periodic Structures,* J. M. Lerner and W. R. McKinney, eds., Proc. Soc. Photo-Opt. Instrum. Eng. **1545,** 241–250 (1991).
12. S. M. Rytov, "Electromagnetic properties of a finely stratified medium," Sov. Phys. JETP **2,** 466–475 (1956).
13. D. L. Brundrett, E. N. Glytsis, and T. K. Gaylord, "Homogeneous layer models for high-spatial frequency dielectric surface-relief gratings: conical diffraction and antireflection designs," Appl. Opt. **33,** 2695–2706 (1994).
14. R. Petit, *Electromagnetic Theory of Gratings* (Springer-Verlag, Berlin, 1980). Chaps. 3 and 4.
15. T. K. Gaylord and M. G. Moharam, "Analysis and applications of optical diffraction by gratings," Proc. IEEE **73,** 894–937 (1985).
16. M. G. Moharam and T. K. Gaylord, "Diffraction analysis of dielectric surface-relief gratings," J. Opt. Soc. Am. **72,** 1385–1392 (1982).
17. M. G. Moharam and T. K. Gaylord, "Rigorous coupled-wave analysis of grating diffraction—*E*-mode polarization and losses," J. Opt. Soc. Am. **73,** 451–455 (1983).
18. D. H. Raquin and G. M. Morris, "Antireflection structured surfaces for the infrared spectral region," Appl. Opt. **32,** 1154–1167 (1993).
19. D. H. Raquin and G. M. Morris, "Analysis of antireflection-structured surfaces with continuous one-dimensional surface profiles," Appl. Opt. **32,** 2582–2598 (1993).
20. R. M. A. Azzam and N. M. Bashara, *Ellipsometry and Polarized Light* (North-Holland, Amsterdam, 1977), Chap. 4.
21. M. K. Moaveni, "Plane-wave diffraction by dielectric gratings, finite difference formulation," IEEE Trans. Antennas Propag. **37,** 1026–1031 (1989).
22. T. Delort and D. Mayestre, "Finite-element method for gratings," J. Opt. Soc. Am. A **10,** 2592–2601 (1993).
23. I. C. Botten, M. S. Craig, R. C. Mcphedran, J. L. Adams, and J. R. Andrewartha, "The dielectric lamellar diffraction grating," Opt. Acta **28,** 413–428 (1981).
24. S. T. Han, Y.-L. Tsao, R. M. Walser, and M. F. Becker, "Electromagnetic scattering of two-dimensional surface-relief dielectric gratings," Appl. Opt. **31,** 2343–2352 (1992).
25. E. N. Glytsis and T. K. Gaylord, "Three-dimensional (vector) rigorous coupled-wave analysis of anisotropic grating diffraction," J. Opt. Soc. Am. A **7,** 1399–1420 (1990).
26. E. N. Glytsis and T. K. Gaylord, "Rigorous 3-D coupled wave diffraction analysis of multiple superposed gratings in anisotropic media," Appl. Opt. **28,** 2401–2421 (1989).
27. E. N. Glytsis and T. K. Gaylord, "Rigorous three-dimensional coupled-wave diffraction analysis of single and cascaded anisotropic gratings," J. Opt. Soc. Am. A **4,** 2061–2080 (1987).
28. N. Chateau and J.-P. Hugonin, "Algorithm for the rigorous coupled-wave analysis of grating diffraction," J. Opt. Soc. Am. A **11,** 1321–1331 (1994).
29. C. W. Haggans, L. Li, and R. K. Kostuk, "Effective-medium theory of zeroth-order lamellar gratings in conical mounting," J. Opt. Soc. Am. A **10,** 2217–2225 (1993).
30. E. N. Glytsis and T. K. Gaylord, "High-spatial-frequency binary and multilevel stairstep gratings: polarization selective mirrors and broadband antireflection surfaces," Appl. Opt. **31,** 4459–4470 (1992).
31. M. E. Motamedi, W. H. Southwell and W. J. Gunning, "Antireflection surfaces in silicon using binary optics technology," Appl. Opt. **31,** 4371–4376 (1992).